3-D Coupled Annular Aperture Antenna Array with Dual Circularly Polarized Isoflux Beam for CubeSat Earth Coverage Applications

Siyu Li, *Student Member*, *IEEE*, Benito Sanz Izquierdo, *Member*, *IEEE*, Shaowei Liao, *Senior Member*, *IEEE*, Quan Xue, *Fellow, IEEE,* Steven Gao, *Fellow, IEEE*

***Abstract*—This communication introduces the concept of coupled annular aperture antenna array (CAAAA) that enhances CubeSat earth coverage with dual circularly polarized (CP) isoflux beams. Unlike the formerly reported annular aperture antenna array (AAAA), which relies on complex feeding networks with numerous excitation ports for amplitude and phase adjustment, the CAAAA simplifies design and reduces radiation losses by optimizing the 3-D spatial arrangement, thus tailoring excitation parameters of passive coupled annular aperture elements encircling a central excitation annular aperture element. The inherent axisymmetric structure of the CAAAA yields a consistent axisymmetric radiation pattern. A C-band (5 GHz) prototype demonstrates ±30° isoflux coverage, 4.5 dBi peak gain, and an axial ratio (AR) beamwidth exceeding 180°, indicating robust dual CP performance. Notable for its low profile (0.11 λ_0), lightweight design, ease of fabrication, and high radiation efficiency, the CAAAA offers a viable, efficient solution for CubeSat applications requiring extensive earth coverage.**

***Index Terms*—antenna array, circular polarization (CP), isoflux beam, earth coverage, CubeSat.**

I. Introduction

Cube Satellites (CubeSats), recognized for their cost-effectiveness, lightweight nature, modular structure, and fabrication simplicity, have predominantly served in low earth orbit (LEO) applications [1, 2]. Many Satellite Communications (SATCOM) applications necessitate shaped radiation patterns, such as isoflux or earth coverage beams, to ensure uniform signal coverage over specific terrestrial areas. These beams compensate for gain loss due to longer propagation distances, thus ensuring stable wireless connections over wide visual areas [3]. Fig. 1 illustrates the necessity for different coverage angles based on satellite heights and coverage areas.

Extensive studies have explored various antenna designs for enhancing satellite communications, particularly in higher orbits like Medium Earth Orbit (MEO) and Geosynchronous Earth Orbit (GEO). Traditional solutions like horn antennas [4], reflector antennas [5], large-scale array antennas [6, 7], helix antennas [8] and choke ring antennas [9-11] have been typically reserved for these applications due to their ability to produce narrow beamwidths. However, their substantial volume and high profile render them unsuitable for deployment on cost-effective, compact CubeSats. Emerging solutions have focused on reducing the physical footprint while maintaining effective coverage [12-14]. For example, a CP patch antenna joint with 12 cross dipole elements demonstrated robust CP isoflux beam performance within a ±60° coverage area at the X band for a 3U-CubeSat [12]. Although effective, the high profile and heavy corrugation of this design are less than ideal for lightweight CubeSat specifications. Another innovative approach involved a patch antenna with a dielectric lens designed to generate an axisymmetric CP isoflux beam with a wide 3-dB AR beamwidth [13]. Nevertheless, the associated bulky dielectric block could hinder practical deployment on lightweight CubeSats. Phased array and time-modulated antenna arrays have also shown potential in simulations, though their development has predominantly remained theoretical, highlighting an area ripe for further exploration and practical implementation [15-19].

Siyu Li and Benito Sanz-Izquierdo are with Division of Computing, Engineering and Mathematical Sciences, University of Kent, Canterbury, UK. (e-mail: sl744@kent.ac.uk, b.sanz@kent.ac.uk)

Steven Gao is with Department of Electronic Engineering, Chinese University of Hong Kong, Hong Kong, China, (email: scgao@ee.cuhk.edu.hk)

Shaowei Liao, Quan Xue are with the School of Electronic and Information Engineering, South China University of Technology, Guangzhou 510641, China. (e-mail: liaoshaowei@scut.edu.cn, eeqxue@scut.edu.cn).

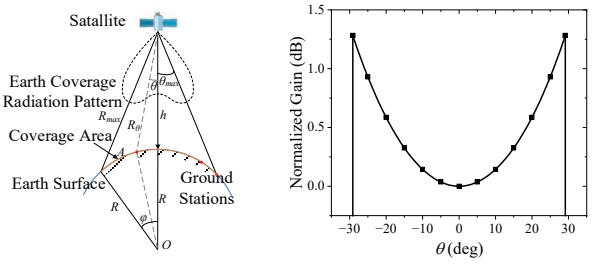

(a) (b)

Fig. 1. (a) 2D cut diagram of the isoflux beam, (b) isoflux mask of a LEO CubeSat with typical operating height and medium-sized country coverage.

Recently, the utility of an annular aperture antenna array (AAAA) was reported, which can create isoflux beams through the adjustment of excitation phase, amplitude, and polarization of its annular aperture elements[14]. This design offers a ±35° CP isoflux coverage, with advantages in terms of weight, profile (0.08 λ_0), and easy CubeSat integration. Despite these benefits, the design's complex feed network introduces significant challenges, resulting in lower radiation efficiency and limited support for polarization, with potential improvements needed in AR beamwidth.

In this communication, the concept of coupled annular aperture antenna array (CAAAA) is introduced and demonstrated. This configuration is achieved by arranging several groups of passive coupled annular aperture elements (coupled AAEs) around a central excitation annular aperture element (excitation AAE). The amplitudes and phases of these AAEs are adjusted by fine-tuning their relative distances and 3-D spatial positioning. Unlike former AAAAs, which require complex feeding networks with numerous excitation ports, the CAAAA simplifies this process. The new array requires only one excitation AAE, significantly reducing design complexity and enhancing radiation efficiency. A prototype designed for C band (5 GHz) is described, which produces a ±30° isoflux beam with dual CP and a broad AR beamwidth. Noteworthy for its low profile (0.11 λ_0), lightweight design, ease of fabrication, and high radiation efficiency, the CAAAA and its prototype stand out as advanced solutions for CubeSat earth coverage applications.

II. Basic Structure and Design Theory of the Coupled Annular Aperture Antenna Array Radiator

Consider a CP isoflux beam AAAA radiator without considering its feeding network, consisting of N AAEs, as shown in Fig. 2 (a) [14]. The aperture refers to the effective area through which an antenna collects or radiates energy [20]. In the following illustrations, the term aperture refers to the annular areas that function as equivalent radiating elements, either through direct excitation or mutual coupling. The concentrically placed AAEs are sequential rotation-fed to achieve a good CP, and the radiation pattern of the overall array could be modulated by controlling the excitation amplitude and

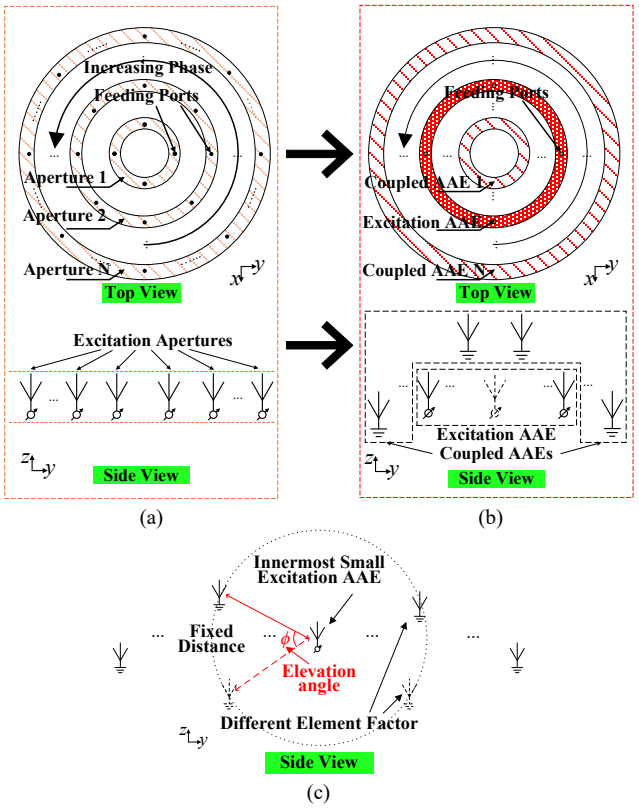

Fig. 2. Evolution from AAAA to CAAAA radiator to achieve CP isoflux beam: (a) AAAA radiator with massive number of feeding ports, (b) proposed CAAAA with much fewer feeding ports, and (c) special case of controlling the coupled AAEs' complex radiation pattern independently.

relative phase of these AAEs. However, this necessitates a substantial number of excitation ports, exemplified by the 12 ports needed for a two-element AAAA radiator in [14], leading to increased complexity of the feeding network. The complex feeding network makes it difficult to reapply in other scenarios and leads to significant transmission loss. Moreover, with more elements introduced, redundancy increases. Additionally, the planar arrangement of AAEs restricts Degrees of Freedom (DoF).

To address the challenge of AAAA, the concept of CAAAA is proposed, as shown in Fig. 2 (b). In this concept, only one of *N* AAEs, namely the excitation AAE, is sequential rotation-fed to produce CP excitation, while the other AAEs are coupled with specific phase and amplitude to achieve isoflux beam for the overall array. This significantly reduces the total number of feeding ports because only one excitation AAE is needed, which greatly simplifies the feeding network and reduces optimization costs. This strategy also makes it possible to achieve CP for the whole array with a single feed port when an innermost centrally single-feed excitation AAE is applied, as shown in Fig. 2 (c). The simplified feeding network and utilizing of the mutual coupling effect also enable a 3D structure, where the coupled AAEs could be placed either above or below the excitation AAE to add more DoFs to the design without notably increasing the overall complexity and optimization cost. Generally, the distance between the coupled and excitation AAEs decides the amplitude and phase of the coupled AAEs, which further determines the synthesized radiation pattern of the overall array.

Assume the radiation pattern is $p_i(\theta,\varphi)$ when only the ith ($i = 1, 2, \dots, N$) AAE is excited by a unit excitation. Consider the case that only the kth ($1 \le k \le N$) AAE is excited, and the other elements are coupled. The amplitude and phase of the ith AAE are denoted as A_i and φ_i, respectively. Based on the superposition principle, the overall radiation pattern of the CAAAA radiator could be given by

$$f(\theta,\varphi) = \sum_{i=1}^{N} A_i e^{j\varphi_i} p_i(\theta,\varphi) \tag{1}$$

where $A_i \in (0,1), i \neq k$, and the amplitude and phase of the kth AAE is $A_k e^{jk} = 1$ as it is excited by a unit power. Typically, the coupled amplitude is less than the excited one and should not be zero, and the phase φ_i already includes the phase introduced by both coupling effect and spacing. Although the coupled AAEs are not directly excited, they still contribute to the radiation due to the mutual coupling effect. This behavior is analogous to Yagi-Uda antenna, where the reflector and director elements radiate as a result of mutual coupling rather than direct excitation. As a result, the $p_i(\theta,\varphi)$ remains applicable for all the AAEs. This equation shows that the guiding ideology of synthesizing the desired beams is to precisely control the coupling amplitude and phase, as well as the relative position of AAEs.

Consider a special case that the excitation AAE is the innermost one ($k = 1$) and its aperture size is relatively small, as shown in Fig. 2 (c). In this ideal case, the coupled amplitude (A_i) and phase (φ_i) should remain constant due to the fixed distance when the ith coupled AAE transforms in a circular orbit within a small elevation angle range (ϕ). However, their contributed radiation pattern $p_i(\theta,\varphi)$ would vary due to the different elevation locations. Notice that the element factor $p_i(\theta,\varphi)$ represents the passive radiation pattern, meaning it is independent of the coupling amplitude and phase but dependent on the structure and position of the ith AAE. This provides a means to independently control the AAEs' complex radiation patterns ($p_i(\theta,\varphi)$ in equation (1)) without affecting their coupled amplitude and phase in specific scenarios. Practical designs benefit from this strategy if the condition mentioned above could be approximately met. Note that this method is not suitable for general cases where the excited AAE is not the innermost one ($k \neq 1$) or is relatively large, but equation (1) still applies and gives a guidance. In general cases, the CP radiation is obtained by sequential rotation-fed technique and a good rotational symmetry is naturally contained in the basic idea of CAAAA, which ensures a good axisymmetric CP shaped beam from the overall array.

III. Design of Coupled Annular Aperture Antenna Array

A. Consideration of the CAAAA Radiator Elements

The proposed CAAAA concept offers an efficient, straightforward, and flexible approach to designing AAAAs. Key design considerations include the selection of the excitation AAE and the arrangement of coupled AAEs. These factors are crucial for achieving the desired CP and isoflux beam performance.

The sequential rotation-fed technique was applied to the excitation AAE to achieve good CP excitation. The excitation AAE can be chosen flexibly based on design requirements. However, using outer AAEs as the excitation AAE would increase the number of feeding ports due to phase difference requirement from sequential rotation-fed technique. This would raise design complexity and transmission loss, as reported in [14]. To streamline analysis and design, the excitation AAE is consistently set to the innermost one in this study. It is important to note that using any AAE as the excitation AAE is feasible in practical scenarios, depending on specific design needs.

To ensure good CP radiation for the overall array, the type of coupled AAEs must be selected carefully. Each coupled AAE needs to support two fundamental orthogonal linearly polarized (LP) modes to generate CP. Commonly used antenna elements capable of generating CP with good rotational axisymmetry such as circular patch antenna, truncated square patch antenna and cross dipole antenna could be considered. While patch antennas can generate CP,

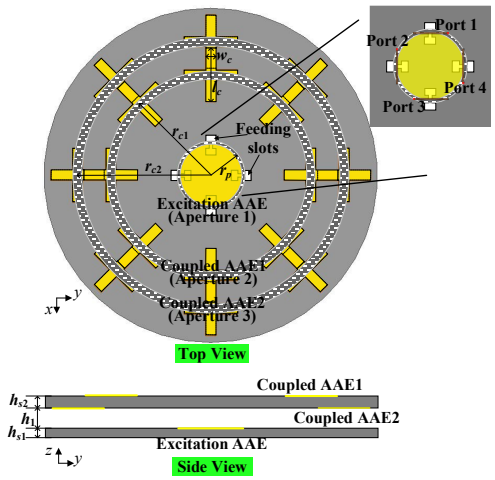

Fig. 3. Configuration of the proposed CAAAA radiator (top and side view). Key parameters: r_p = 9.75 mm, r_{c1} = 30 mm, r_{c2} = 40 mm, l_c = 16 mm, w_c = 3mm, $h_{s1} = h_{s2}$ = 1.524mm, h_1 = 3 mm.

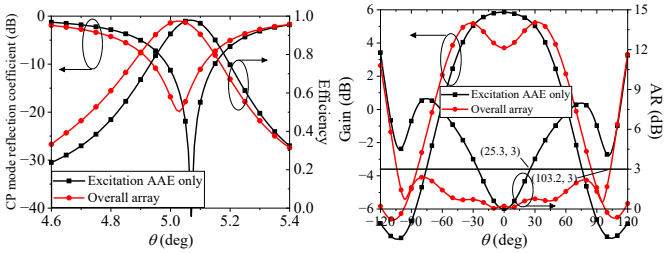

(a) (b)

Fig. 4. Performance with and without coupled AAEs. (a) CP mode reflection coefficient and efficiency, and (b) radiation pattern and AR.

they require adequate distance from the ground plane to resonate and radiate properly. This requirement makes them unsuitable for the flexible 3-D positioning needed in CAAAA designs. Therefore, cross dipole elements were applied due to their advantages of both good CP performance and flexibility of changing the position. By strategically selecting and positioning the excitation and coupled AAEs, the CAAAA can achieve efficient CP isoflux beam performance with reduced design complexity.

B. Radiator Design

For a clearer demonstration of the proposed concept and design theory, a CAAAA radiator capable of producing a dual CP isoflux beam was simulated, reflecting conditions typical of LEO satellites. The technical specifications were determined for satellites operating at altitudes (h) of 500 km with coverage areas (A) of 250,000 km². This scenario depicts typical CubeSat LEO satellite coverage over a medium-sized country. Fig. 1 (b) displays the corresponding isoflux mask, calculated according to [21]. The calculated maximum gain direction is located at $\theta_{max} = \pm 29.1°$ and relative gain at θ_{max} is 1.28 dB higher compared to that of broadside direction. The specifications listed below are based on the defined isoflux mask and practical requirements:

- Frequency: 5 GHz ± 50 MHz
- Footprint Size: Ø100 mm (1U CubeSat mounting face)
- Profile: the lower the better
- Polarization: dual CP (LHCP/ RHCP)
- AR: ≤ 3 dB within $\theta = \pm 50°$
- Gain: > 2 dBic @$\theta = 0°$, and > 4 dBic @$\theta = \pm 30°$
- Efficiency: ≥ 80%

The designed CAAAA radiator shown in Fig. 3 compromises three AAEs, with the innermost one being a circular patch antenna

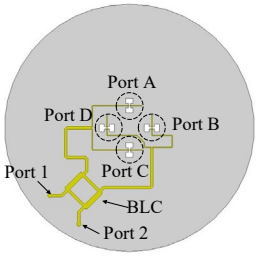

Fig. 5. Configuration of the dual CP feeding network.

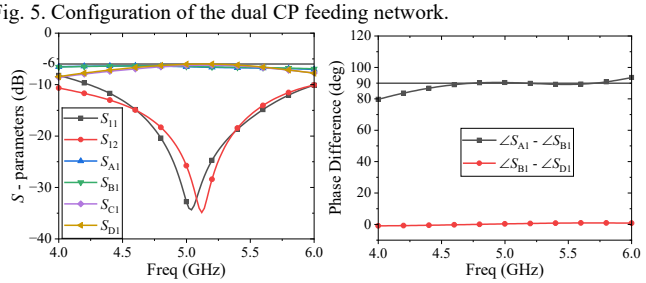

(a) (b)

Fig. 6. Simulated single-ended S-parameters of the feeding network. (a) reflection, isolation, and transmission coefficient, (b) phase difference.

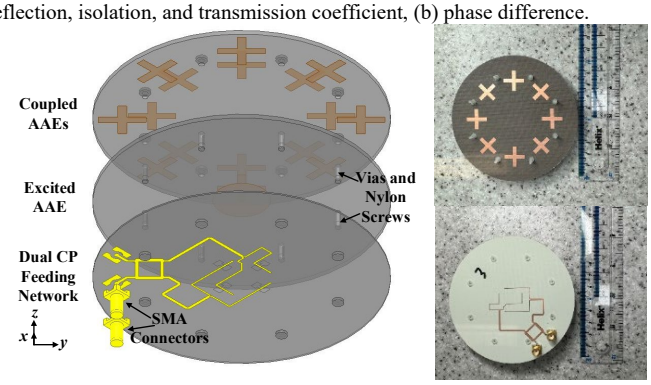

(a) (b)

Fig. 7. 3-D exploded view and photos of the fabricated prototype, (a) 3-D exploded view, (b) top and bottom view.

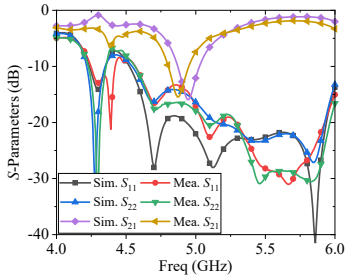

Fig. 8. Simulated and measured S-parameters of the prototype.

sequential rotation-fed to provide CP excitation. The remaining two coupled AAEs are formed by two cross dipole aperture elements, each comprising eight cross dipole elements rotationally placed to synchronize with the sequential rotation-fed CP patch antenna. All cross dipole elements share identical dimensions in length and width. The coupled AAEs are situated on both sides of the substrate, with the substrate thickness determining the height difference between these two coupled AAEs. Based on the theoretical analysis outlined in Section II, the relative position, the coupled amplitude and phase of the coupled AAEs could be modified by properly varying the height difference (h_1, h_{s2}) and radius (r_{c1}, r_{c2}), between the excitation and coupled AAEs, enabling isoflux beam for the entire array.

The substrate applied for both excitation and coupled AAEs is Rogers Arlon AD255C laminate ($\varepsilon_r = 2.55$, $\tan\delta = 0.0014$). The planar dimension of all substrates and ground plane were set to Ø100

mm to fit into a standard 1U CubeSat mounting surface (100 mm × 100 mm) and ensure an axisymmetric radiation performance. The circular patch is coupled fed by two sets of slots to produce two orthogonal TM_{11} modes and provide an axisymmetric CP radiation along φ direction from its aperture.

Since the single ended *S*-parameters are not applicable for multi-port radiators, the CP mode, instead of single-ended reflection coefficient, is applied to evaluate the matching performance of the sequential rotation-fed radiator, using the method proposed in [22]. This method applies the multi-mode *S*-parameters to provide a clear physical insight and provide an intuitive, direct way to evaluate the matching performance of a multi-port radiator without calculating the complex far field. The left-hand circular polarization (LHCP) and right-hand circular polarization (RHCP) mode reflection coefficients are given by,

$$S_{LL} = S_{RR} = S_{11} - S_{31}. \quad (2)$$

where S_{LL}, S_{RR} represent the LHCP and RHCP mode reflection coefficient, respectively, and subscripts 1 - 4 represent the four excitation ports for the sequential rotation-fed radiator, as shown in Fig. 3. S_{LL} (S_{RR}) indicates the amount of energy reflected by LHCP (RHCP) mode radiation, therefore reflecting the efficiency of LHCP (RHCP) mode radiation from this radiator. By properly optimizing S_{11} and S_{31} through the strategic arrangement of the position and shape of the feeding slots, both S_{LL} and S_{RR} can be minimized, indicating efficient LHCP and RHCP radiation from this radiator.

All the AAEs are optimized to work at 5 GHz, and the corresponding key parameters are given in the caption of Fig. 3. The matching and radiation performance are shown in Fig. 4. Due to the symmetry of the structure, only the results at $\varphi = 0°$ plane for radiation patterns are given for concision in the following illustrations. As can be seen Fig. 4 (a), a consistency between the total efficiency and CP mode reflection coefficient is observed, and the good CP mode reflection coefficient means that both structures work well at 5 GHz. The total efficiency remains above 97% for both structures, proving that a good matching performance is achieved. As shown in Fig. 4 (b), the radiation pattern was shaped from a conventional pencil beam to an isoflux form when the coupled AAEs were introduced, while the peak gain remains 5.3 dBi at φ = 31°. A significant improvement for axial ratio (AR) from ±25° to ±103° is observed, making it possible to cover the area within angular range of over 200°. All the results prove a good isoflux beam radiation and AR beamwidth improvement of the designed structure and the feasibility of the proposed concept.

C. Feeding Network Design

The feeding network achieving dual CP is shown in Fig. 5. It consists of two input ports, namely Port 1 and Port 2, which correspond to RHCP, LHCP mode excitation input, respectively. The key component of this network is a branch line coupler (BLC, or also known as 3-dB hybrid coupler). The BLC could guarantee a 90° phase difference at its two output ports. Depending on which input port is used, the network can achieve either a 90° or -90° phase shift, corresponding to the two different CP modes required to feed the radiator.

The performance of the dual CP feeding network is evaluated using single-ended *S*-parameters, as shown in Fig. 6. Due to the symmetry of the BLC, only the results for RHCP input port (port 1) are given, with the results for the LHCP input port (port 2) being similar. Benefiting from the merit of BLC, good reflection from input ports was observed, both better than -30 dB within working band. Additionally, a transmission coefficient approaching -6 dB within the band confirms the efficacy of the dual CP feeding network. The phase

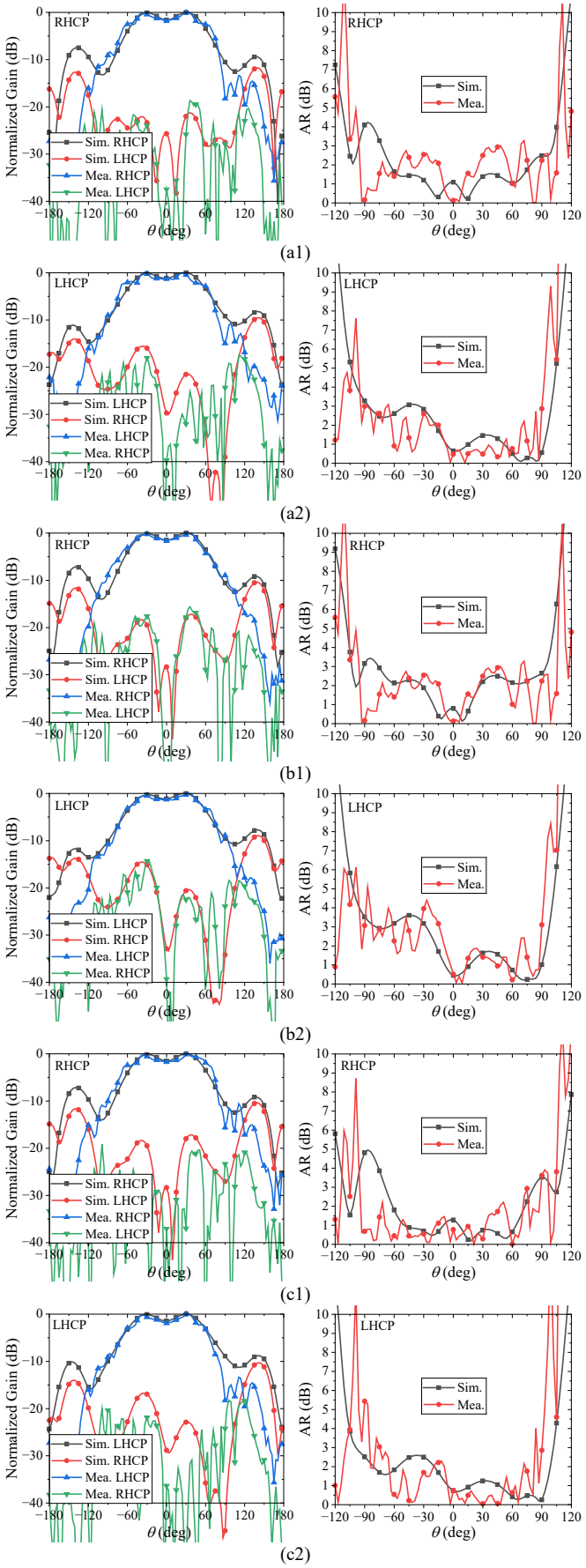

Fig. 9. Simulated and measured radiation pattern and spatial AR at (a) 5 GHz, (b) 4.95 GHz, and (c) 5.05 GHz.

Table I. COMPARISON BETWEEN THE PROPOSED ANTENNA AND COUNTERPARTS WITH ISOFLUX BEAM FOR EARTH COVERAGE APPLICATIONS

Ref.	Technique	Application	Isoflux Angle	Peak/ Broadside Gain (dBi)	Polarization	3-dB AR Beamwidth	Dimension	Remarks
[4]	Reflector	GEO	±14°	16/13.8	LP	\	Ø6.5 λ_0 × 22.3 λ_0	high gain, high profile, heavy, LP
[23]	PRS	LEO	±17°	~17.5/~15	LP	\	Ø5.5 λ_0 × 5 λ_0	high gain, huge size, high profile, LP
[8]	Helix	LEO	±90°	3.3/~0	CP	~240°(5dB)	1 λ_0× 1λ_0×1.47λ_0	wide beamwidth, high profile, bulky
[17]	Phased array	LEO CubeSats	~ ±17°	11.5/~11	CP	50°	Ø5.5 λ_0×0.053 λ_0, (only radiator)	for CubeSat application, only simulation of radiator, no prototype
[13]	Lens	LEO CubeSats	±50°	3.45/≥ -5	CP	140°	1.67 λ_0×1.67 λ_0× 0.59 λ_0	for CubeSat application, bulky dielectric block
[14]	AAAA	LEO CubeSats	±35°	3.48/0.87	CP	110°	1.67 λ_0×1.67λ_0 × 0.078 λ_0	for CubeSat application, low profile, light weight
This work	CAAAA	LEO CubeSats	±30°	4.5/2.7	Dual CP	180°	Ø1.67 λ_0×0.11 λ_0	for CubeSat application, low profile, higher gain, wider AR beamwidth

* Exclude SMA

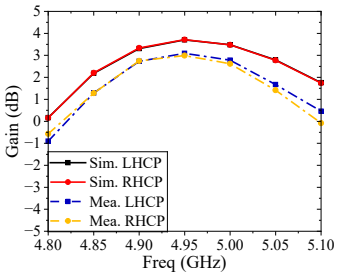

Fig. 10. Simulated and measured broadside gain of the proposed antenna.

response at output ports shows that a good 90° phase difference is obtained, which ensures a good CP excitation for the radiator.

IV. FABRICATION AND MEASUREMENT

To demonstrate the practical viability of the proposed CAAAA design, a prototype was fabricated and evaluated. The exploded view of the structure and photos of the fabricated antenna are shown in Fig. 7. To ensure proper alignment and robustness of the structure, eight pairs of nylon vias and screws were added. Corresponding 8 × 3 mm spacers were used to maintain the vertical distance between the excitation and coupled AAEs. The overall dimensions of the fabricated prototype are Ø100 mm × 6.556 mm (Ø1.6 λ_0 × 0.11 λ_0, excluding the SMA connector). The reflection coefficient and the far field performance of the prototype were measured using Keysight P9377B network analyzer and an anechoic chamber system, respectively. A foam absorber backing was added to minimize the impact of metal back reflection on the front radiation pattern.

The simulated and measured *S*-parameters are depicted in Fig. 8. As can be seen, the simulated and measured results of two input ports are generally matched, where the -10-dB bandwidth is 4.57 – 6.06 GHz. Notably, the cross-coupling exceeds -10 dB at 5 GHz. Therefore, the proposed antenna is more suitable for switchable dual-CP scenarios, ensuring high cross-coupling does not impact normal system operation. However, this limitation can be addressed using multi-stage BLCs or advanced high-performance wideband BLCs. With these enhancements, the antenna could operate in LHCP and RHCP modes simultaneously, thereby increasing power capacity.

The simulated and measured radiation performance are shown in Fig. 9. Due to the rotational axisymmetry of the structure, only the results at $\varphi = 0°$ is plotted. For antennas producing an isoflux radiation pattern for SATCOM applications, spatial AR performance is preferred over AR bandwidth at the broadside direction due to space coverage characteristics. As shown in Fig. 9, the measured radiation patterns closely match with the simulated ones in both RHCP and LHCP cases when different input ports were excited. A 3-dB AR beamwidth exceeding 180° was observed at 5 GHz, specifically -95° ~ 105° for RHCP and -94° ~ 90° for LHCP excitation, as shown in Fig. 9 (a). Similar performance could be observed in most cases shown in Fig. 9 (b) and (c), where a stable isoflux radiation pattern and 3-dB AR beamwidth exceeding 180° could be achieved. The measured realized gain at broadside direction is generally 0.7 dB lower than the simulated result, where a 2.7 dB measured realized gain at 5 GHz is observed in Fig. 10. The measured gain loss is mainly attributed to the feeding network cascade and manufacturing errors, which are within an acceptable range. Overall, the prototype meets the performance requirements, demonstrating the feasibility and robustness of the proposed CAAAA design.

V. DISCUSSION

A comparison between the proposed antenna with previously reported counterparts is present in Table II, listing only the most relevant ones for brevity. In contrast to conventional large-scale antenna arrays and high-profile horn antennas tailored for GEO satellites [4], the proposed antenna provides an cost-effective solution for miniatured satellites like CubeSats, delivering dual CP isoflux performance. Unlike the helix antenna with high profile [8] and choke ring antenna with heavy metal [9] to produce isoflux beam, the proposed antenna could provide a light-weight, low-profile alternative with dual CP isoflux radiation pattern capabilities. Compared to patch antenna with a bulky dielectric block as lens for beam shaping, the proposed antenna utilizes commonly used commercial laminates, significantly reducing dimension and cost of the whole structure. Notably, compared with the AAAA proposed in [14], a key parameter that matters in SATCOM applications, namely AR beamwidth is greatly improved greatly without increasing the volume and cost of the structure. Furthermore, the proposed CAAAA concept's inherent advantages include high DoFs afforded by efficient utilization of 3D space, a simplified feeding network structure that leads to reduced insertion loss and higher efficiency, and consequently, a higher peak gain. These attributes collectively enhance the practical applicability of the design for various applications. Nonetheless, the proposed idea can be easily adapted to other beam shaping applications to generate various applicable patterns. The proposed antenna has a power capacity of about 10-watt level, and thus is suitable for CubeSat earth coverage applications, such as telemetry, tracking and command (TT&C), and low-speed communication. The gain of the proposed antenna is not comparable to those with large apertures, because the design is for CubeSat TT&C and low-speed communication applications, where maintaining a compact size, and stable and

continuous signal transfer over a broad area is more critical. The proposed design operates at 5 GHz, but its design method is applicable to other C-band frequencies, widely used in SatCom applications, such as remote sensing and TT&C communications [24-26]. However, due to the size constraints of CubeSats, this design approach is more suitable for relatively higher frequency bands. This is because that effective beam shaping requires a sufficiently large aperture, making it challenging to design a shaped-beam antenna for lower bands (such as L and S) on a CubeSat, regardless of the method used.

Considering CubeSat integration, a stripline-based feeding network will offer an effective solution to minimize the profile increase and ensure optimal electrical performance. For instance, a 0.5 mm-wide stripline placed between two Rogers 4350B substrates (each 0.508 mm thick) results in a total feeding network height of 1.016 mm with 50-ohm impedance. This approach will ensure a compact, low-profile design that maintains compatibility with CubeSat requirements and addresses the integration challenges of open microstrip lines. Although only the results for the standalone structure were presented in the manuscript, cases of the proposed structure mounted on 1U and 2U CubeSat bodies were also considered and simulated. The simulation results showed that the CubeSat body has a minimal impact on the antenna's performance.

VI. Conclusion

This paper presents a novel dual CP isoflux beam antenna for CubeSat earth coverage applications, based on the concept of a coupled annular aperture antenna array (CAAAA). Unlike traditional annular aperture antenna arrays, the proposed CAAAA structure achieves beam shaping with a simpler feeding network, reduced insertion loss, higher efficiency, and greater design flexibility due to its 3D layout capability. A prototype operating at C-band (5 GHz) was designed, fabricated, and tested, showing a ±30° isoflux coverage, 4.5 dBi peak gain, and an AR beamwidth exceeding 180°. The low-profile (0.11 λ_0), lightweight, and easy-to-integrate design makes it highly suitable for CubeSat applications requiring extensive earth coverage. Additionally, the CAAAA concept can be adapted for various beam shaping applications, demonstrating its versatility and potential for future satellite communication systems.

References

[1] W. Shiroma *et al.*, "CubeSats: A bright future for nanosatellites," *Open Engineering,* vol. 1, no. 1, pp. 9-15, 2011.

[2] S. Zarbakhsh, M. Akbari, M. Farahani, A. Ghayekhloo, T. A. Denidni, and A. Sebak, "Optically transparent subarray antenna based on solar panel for cubeSat application," *IEEE Transactions on Antennas and Propagation,* vol. 68, no. 1, pp. 319-328, 2020, doi: 10.1109/TAP.2019.2938740.

[3] W. A. Imbriale, S. S. Gao, and L. Boccia, *Space Antenna Handbook*. John Wiley & Sons, 2012.

[4] A. Love, "Two hybrid mode, earth coverage horn for GPS," in *1985 Antennas and Propagation Society International Symposium*, 1985, vol. 23, pp. 575-578.

[5] S. Hay, D. Bateman, T. Bird, and F. Cooray, "Simple Ka-band earth coverage antennas for LEO satellites," in *IEEE Antennas and Propagation Society International Symposium. 1999 Digest. Held in conjunction with: USNC/URSI National Radio Science Meeting (Cat. No. 99CH37010)*, 1999, vol. 1, pp. 708-711.

[6] A. Montesano *et al.*, "Galileo system navigation antenna for global positioning," in *The Second European Conference on Antennas and Propagation, EuCAP 2007*, 11-16 Nov. 2007 2007, pp. 1-6, doi: 10.1049/ic.2007.1441.

[7] G. Minatti, S. Maci, P. De Vita, A. Freni, and M. Sabbadini, "A circularly-polarized isoflux antenna based on anisotropic metasurface," *IEEE Transactions on Antennas and Propagation,* vol. 60, no. 11, pp. 4998-5009, 2012.

[8] M. Taherkhani, J. Tayebpour, S. Radiom, and H. Aliakbarian, "Circularly polarised wideband quadrifilar helix antenna with ultra-wide beamwidth isoflux pattern for a S-band satellite ground station," *IET Microwaves, Antennas & Propagation,* vol. 13, no. 10, pp. 1699-1704, 2019.

[9] M. Fallahzadeh, H. Aliakbarian, A. Haddadi, and S. Radiom, "Beam shaping of X-band stepped choke ring antenna for LED satellite applications," *IEEE Aerospace and Electronic Systems Magazine,* vol. 33, no. 10, pp. 34-39, 2018.

[10] E. Taghdisi, M. S. Ghaffarian, and R. Mirzavand, "Low-Profile Substrate Integrated Choke Rings for GNSS Multipath Mitigation," *IEEE Transactions on Antennas and Propagation,* vol. 70, no. 3, pp. 1706-1718, 2022-03-01 2022, doi: 10.1109/tap.2021.3118809.

[11] E. Arnaud *et al.*, "Compact Isoflux X-Band Payload Telemetry Antenna With Simultaneous Dual Circular Polarization for LEO Satellite Applications," *IEEE Antennas and Wireless Propagation Letters,* vol. 19, no. 10, pp. 1679-1683, 2020-10-01 2020, doi: 10.1109/lawp.2020.3013989.

[12] J. Fouany *et al.*, "New concept of telemetry X-band circularly polarized antenna payload for CubeSat," *IEEE Antennas and Wireless Propagation Letters,* vol. 16, pp. 2987-2991, 2017.

[13] X. Ren, S. Liao, and Q. Xue, "A Circularly Polarized Spaceborne Antenna with Shaped Beam for Earth Coverage Applications," *IEEE Transactions on Antennas and Propagation,* vol. 67, no. 4, pp. 2235-2242, 2019, doi: 10.1109/TAP.2018.2889188.

[14] S. Li, S. Liao, Y. Yang, W. Che, and Q. Xue, "Low-Profile Circularly Polarized Isoflux Beam Antenna Array Based on Annular Aperture Elements for CubeSat Earth Coverage Applications," *IEEE Transactions on Antennas and Propagation,* vol. 69, no. 9, pp. 5489-5502, 2021-09-01 2021, doi: 10.1109/tap.2021.3060039.

[15] M. Ibarra, A. G. Andrade, M. A. Panduro, and A. L. Mendez, "Design of antenna arrays for isoflux radiation in satellite systems," in *2014 IEEE 33rd International Performance Computing and Communications Conference (IPCCC)*, 5-7 Dec. 2014 2014, pp. 1-2, doi: 10.1109/PCCC.2014.7017028.

[16] L. I. Balderas, A. Reyna, and M. A. Panduro, "Time-modulated concentric ring antenna array for a wide coverage pattern," in *2016 IEEE International Symposium on Antennas and Propagation (APSURSI)*, 26 June-1 July 2016 2016, pp. 709-710, doi: 10.1109/APS.2016.7696063.

[17] J. E. Diener, R. D. Jones, and A. Z. Elsherbeni, "Isoflux phased array design for cubesats," in *2017 IEEE International Symposium on Antennas and Propagation & USNC/URSI National Radio Science Meeting*, 2017, pp. 1811-1812.

[18] X. Ren, B. Wang, and H. Wong, "Field manipulation by a dielectric block for partial isoflux radiation," *Applied Physics Express,* vol. 13, no. 2, p. 021001, 2020, doi: 10.35848/1882-0786/ab6ca4.

[19] A. Reyna, L. I. Balderas, and M. A. Panduro, "Time-modulated antenna arrays for circularly polarized shaped beam patterns," *IEEE Antennas and Wireless Propagation Letters,* vol. 16, pp. 1537-1540, 2017.

[20] Balanis, *Antenna Theory Analysis and Design.3rd Edition*.

[21] M. Cai, W. Li, X. Shi, Q. Zhang, H. Liu, and Y. Li, "An Innovative Design of Isoflux Scanning Digital Phased Array Based on Completely Shared Subarray Architecture for Geostationary Satellites," *Electronics,* vol. 12, no. 18, p. 3850, 2023-09-12 2023, doi: 10.3390/electronics12183850.

[22] S. Li, S. Liao, W. Che, and Q. Xue, "Generalized Multimode Scattering Parameters and the Applications in Antenna and Radio Frequency Component Designs," *International Journal of RF and Microwave Computer-Aided Engineering,* vol. 32, no. 11, 2022-11-01 2022, doi: 10.1002/mmce.23392.

[23] C. Abella, J. Peces, M. Marín, J. Martinez, and K. Markus, "Development of a compact antenna for global earth coverage," in *1993 23rd European Microwave Conference*, 1993, pp. 906-908.

[24] M. Wei and D. T. Sandwell, "Decorrelation of L-Band and C-Band Interferometry Over Vegetated Areas in California," *IEEE Transactions on Geoscience and Remote Sensing,* vol. 48, no. 7, pp. 2942-2952, 2010-07-01 2010, doi: 10.1109/tgrs.2010.2043442.

[25] N. Baghdadi, M. Bernier, R. Gauthier, and I. Neeson, "Evaluation of C-band SAR data for wetlands mapping," *International Journal of Remote Sensing,* vol. 22, no. 1, pp. 71-88, 2001-01-01 2001, doi: 10.1080/014311601750038857.

[26] Hasituya, Z. Chen, F. Li, and Hongmei, "Mapping Plastic-Mulched Farmland with C-Band Full Polarization SAR Remote Sensing Data," *Remote Sensing,* vol. 9, no. 12, p. 1264, 2017-12-06 2017, doi: 10.3390/rs9121264.